ORIGINAL RESEARCH ARTICLE

Current observations from a looking down vertical V-ADCP: interaction with winds and tide? The case of Giglio Island (Tyrrhenian Sea, Italy)

Laura Cutroneo [a], **Gabriele Ferretti** [a], **Davide Scafidi** [a],
Gian Domenico Ardizzone [b], **Greta Vagge** [a], **Marco Capello** [a,*]

[a] *DISTAV, University of Genoa, Genoa, Italy*
[b] *"Sapienza", University of Rome, Rome, Italy*

Summary   In the context of the environmental monitoring of the Concordia wreck removal project, measurements of currents, winds and sea level height were made along the eastern coast of the Giglio Island, Tyrrhenian Sea (Italy), during 2012—2013. The aim of the study was to investigate the effect of atmospheric forcing and periodic sea-level changes on the coastal currents. Normalised Cross-Correlation Function analysis allowed us to correlate these observations. A marked inter-seasonal variability was found in both current and local wind velocity observations but a significant level of correlation between the data was only found during strong wind events. Current and wind directions appeared to be uncorrelated and current measurements showed a predominant NW—SE direction, presumably linked to the shape and orientation of Giglio Island itself. During strong winds from the SSE, current flow was towards the NNW but it suddenly switched from the NNW to the SE at the end of wind events. The results show that, at Giglio Island, currents are principally dominated by the general cyclonic Tyrrhenian circulation, and, secondly, by strong wind events. The sea level had no effects on the current regime.

---

 * Corresponding author at: DISTAV, University of Genoa, 26 Corso Europa, I-16132 Genoa, Italy. Tel.: +39 01035338143; fax: +39 010352169.
   E-mail address: capello@dipteris.unige.it (M. Capello).

1. Introduction

Sea and ocean circulation is generally characterised by the interactions of tidal currents, bathymetric constraints, wind forcing, and density gradients induced by river input and heat and mass (evaporation and rain) exchange. In this complex scenario, wind has been found to be the main forcing factor inducing currents, while tidal and baroclinic motions are of secondary importance (Bolaños et al., 2014). The barotropic component of the coastal circulation is mainly driven by local winds, but is also highly dependent on the topography of the marine basin, composed of sub-basin scale gyres that can be seasonally variable and recurrent (Molcard et al., 2002; Pierini and Simioli, 1998).

The periodic vertical motions produced by tides close to the coast induce (horizontal) currents with alternating floods and ebbs. In these water movements, tides can have local or regional and short-range or long-range influences (Naranjo et al., 2014). Close to the coast, sea level depends primarily on the periodic change of lunar and solar attraction (astronomic influences), but also on the local atmospheric pressure and wave and wind changes (atmospheric events) that induce non-periodic signals of varying strength (amplitude) and duration (low-frequency) which influence the daily periodic oscillations (Halverson, 2014; Tsimplis et al., 2011). Moreover, the magnitude of the sea level variation is site dependent. In fact, in areas characterised by very small tidal ranges, such as the Mediterranean Sea, the atmospheric effects may have greater amplitude than the normal tide and can partially or completely obscure the astronomic tide oscillations. These atmospheric effects vary, for example, with the direction, strength and duration of the wind and are also dependent on the morphology of the area and the depth of the body of water (Halverson, 2014).

In the context of the environmental monitoring of the Concordia wreck removal project, measurements of currents, winds and sea level were made during 2012—2013 along the eastern coast of the Giglio Island in the Tyrrhenian Sea (Italy) (Fig. 1). In order to study the general trend of the currents, and their daily and seasonal variations in relation to atmospheric forcing (winds) and periodic sea level changes (tides), a vertical Acoustic Doppler Current Profiler (V-ADCP) was deployed under a buoy from the 29th August 2012 to the 7th July 2013. The results of the cross-correlation analysis of the continuous data collected by the V-ADCP and the meteorological (wind velocity and direction) and sea level observations recorded at the permanent weather station of Giglio Porto are reported in this paper.

2. Study area

2.1. Geological and climatic characteristics of Giglio Island

Giglio Island (21.2 km^2) lies in the northern part of the Tyrrhenian Sea in front of the Argentario headland, 14-km off the Tuscany coast (Fig. 1). The small town and the harbour of Giglio Porto are on the eastern side of the island (Fig. 1). The island is 90% composed of a monzogranitic pluton resulting from crystallisation of magma within the earth's crust and raised to the surface as a result of a tectonic extensional phase subsequent to the collision between the Adriatic and Corsica-Sardinia plates (Rossetti et al., 1999). The island's shape is roughly elliptical, 8.5 km long and 4.5 km wide, with its major axis oriented NNW-SSE. Its coasts are predominantly high and rocky with numerous small bays and inlets. The sea bottom off the Giglio Porto coast is characterised by a steep rocky slope that slopes quickly to a 100-m depth at a distance of about 350 m from the coast. Sea bottom, beneath 50-m depth, consists of more than 60% clay (Frezza and Carboni, 2009).

The island's climate is typically Mediterranean, with rare rainfall between May and October (almost completely absent
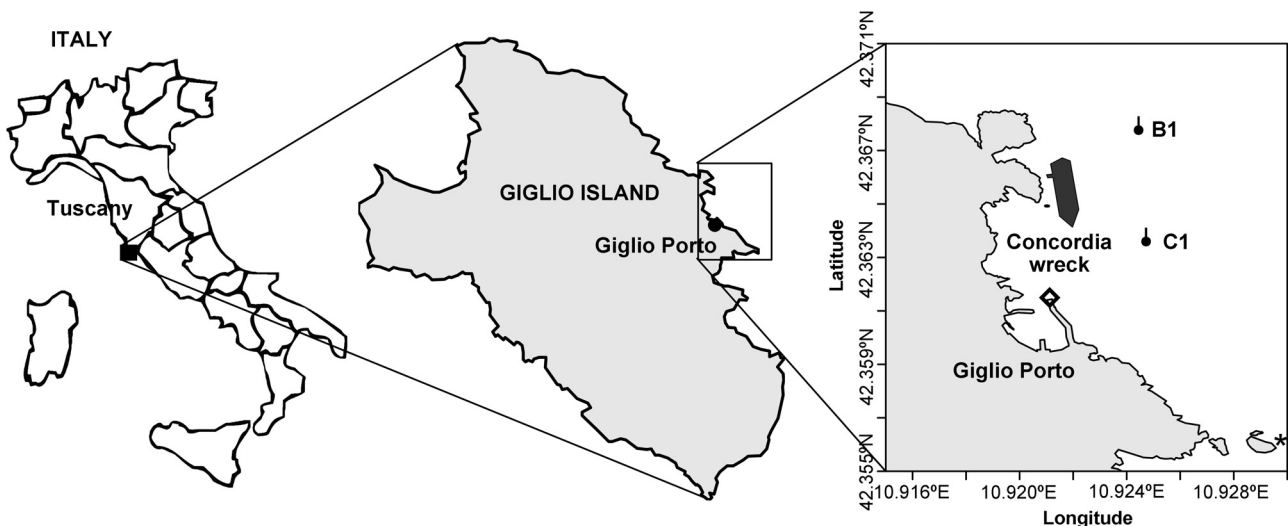
Figure 1 Location of the study area (Giglio Island, Italy). B1 and C1 are the buoys under which the V-ADCP was installed for the continuous monitoring of the currents; Concordia wreck black profile highlights the position of the vessel near the coast off Giglio Porto; the black rhombus shows the position of the weather station of the LaMMA Consortium (Environmental Modelling and Monitoring Laboratory for Sustainable Development) of the Tuscany Region; the black asterisk shows the collision point of the cruise vessel on the rocks.

in the summer months), and more frequent rainfall between November and April. The temperature is relatively mild in winter (minima > 0°C) and high in summer (maxima > 30°C). The weather conditions of the island are mostly influenced by wind action; in particular, the winds from the SE, S, SW and NE are linked with rains, while the winds from the NW, W and N are linked with dry weather. The N and NE winds typically blow during winter (December, January, and February) and can produce storms, while, in autumn and spring, strong SE and S—SW winds generate rough seas, principally on the southern and eastern coasts of the island. In summer, the dominant wind is from the S and of low velocity, generally associated with calm seas (http://www.cmgizc.info).

2.2. The circulation and tides in the Tyrrhenian Sea

The study area is included in the general circulation of the Tyrrhenian Sea. This circulation is characterised by surface and intermediate layers represented by a well-defined flux of Atlantic Water (AW; the Tyrrhenian vein) entering the basin from the south along the eastern coast of Sicily and flowing counter-clockwise around the Tyrrhenian and northward along the Italian peninsula reaching the Channel of Corsica. Here, a part of the flow enters the Ligurian Sea, while another part moves in a cyclonic gyre off the Boniface Strait (Astraldi and Gasparini, 1994; Millot and Taupier-Letage, 2005; Vetrano et al., 2010). When the Tyrrhenian vein of the AW reaches the channel between Giglio Island and the Italian coast, currents are forced in an SE—NW direction, disturbed by gyres and counter-current induced by the inter-action with the coastal morphology, friction with the shallow bottom, and the influence of the freshwater inputs from torrents and rivers. This situation was highlighted in satellite picture taken on the 13th November 2012 after heavy rains that hit the region (Fig. 2; source NASA).

The Tyrrhenian circulation suffers from some important seasonal changes, primarily in the northern part of the basin. Here, the water masses are mostly recirculated within the basin in summer, isolating the Tyrrhenian and Ligurian seas, with only a small part of the flow passing through the Corsica Channel; in winter and spring, the communication between the two basins is full (Astraldi and Gasparini, 1994; Pierini and Simioli, 1998; Schroeder et al., 2011).

In general, the maximum tidal range is relatively low in the Tyrrhenian Sea, equal 0.45 m (Ferrarin et al., 2013). Tidal

Figure 2 Evidence of the current coastal gyres produced by coast morphology and fresh water input from rivers. Satellite picture taken on the 13th November 2012 after heavy rains. Source: NASA.

oscillations (Table 1) are semidiurnal, with two highs and two lows during the day, which occur with different values during the year producing minor and major tides that are strongly correlated with the mean surface pressure variations; sea-sonal fluctuations have a progressive increase and sharp decrease, with the maximum signal in autumn (Mosetti and Purga, 1982; Polli, 1955). The mean sea level curve is dominated by a strong annual signal of 8 cm in amplitude (Cazenave et al., 2002).

Table 1 Mean tidal semi-diurnal and diurnal harmonic constituents (M2, S2, K1, and O1) expressed in amplitude (in cm) and phase (in degree, °) at the tidal gauge of the Civitavecchia harbour during the period 1951—1952 (Polli, 1955). Solar annual component (Sa), solar semi-annual component (Ssa), solar monthly component (MSm), and lunar monthly component (Mm) at the tidal gauge of the Civitavecchia harbour during the period 1966—1968 (Mosetti and Purga, 1982).

Polli (1955)	M2 (the principle lunar semi-diurnal harmonic)	S2 (the principle solar semi-diurnal harmonic)	K1 (the principle luni-solar diurnal component)	O1 (the principle lunar diurnal component)
Period 1951—1952	10.9 cm, 258°	4.1 cm, 280°	2.8 cm, 202°	1.3 cm, 115°
Mosetti and Purga (1982)	Sa (solar annual component)	Ssa (solar semi-annual component)	MSm (solar monthly component)	Mm (lunar monthly component)
Period 1966—1968	5.6 cm, 216°	3.4 cm, 111°	0.8 cm, 276°	0.3 cm, 246°

3. Material and methods

The signal buoys delimiting the marine yard of the Concordia wreck removal project were located 300—500 m off Giglio Porto (Fig. 1) at the 80—100 m isobaths. The buoys (Resinex Trading Srl) were manufactured with an external shell in roto-moulded linear polyethylene and filled with elastomer polyurethane to guarantee buoyancy.

A Teledyne RDI 300-kHz downward-looking vertical four-beam V-ADCP was installed under buoy C1 on the 29th August 2012 and moved to buoy B1 on the 25th November 2012, at a fixed depth of 6 m to continuously monitor the currents. The 6-m depth was chosen because of the shape of the buoy, equipped with a pipe in its submerged part. The V-ADCP was powered by an internal battery pack and installed on the buoy cable with a stainless steel structure that avoided beam interaction with the cable itself. The instrument was equipped with an armoured submarine cable with a terminal above sea level from which data were downloaded.

The V-ADCP could measure current profiles (velocity and direction) and the intensity of the echo (backscatter) along a theoretical vertical line of about 120 m (RD, Instruments 2007) from the depth of installation (6 m) to the sea bottom. The size of V-ADCP bins was set at 4 m and the maximum number of bins at 16, to cover 70 m of the water column, and, hence, the first measurement bin was centred at a 10-m depth. The instrument measured the velocity [mm s^{-1}] and direction [°N] of the current with a sampling of 6 min averaging 30 pings for each measurement (1 ping every 12 s).

The measurement period lasted from the 29th August 2012 till the 7th July 2013, but it was divided into sub-periods of non-equal duration depending on yard operations and weather conditions (Table 2). From the 29th August to the 25th November 2012, the instrument was fixed under buoy C1 (Fig. 1), but, due to the frequent removals and repositioning of the buoy for the manoeuvres of tugs and pontoons engaged in the yard operations, it was successively (from 25th November 2012) fixed under buoy B1 (Fig. 1) (Table 2) situated 800 m to the North.

The software used for the V-ADCP configuration and the data downloading was WinSC (RD Instruments, Inc.), while the software used for data processing was WinADCP (RD Instruments, Inc.).

Following the oceanographic convention, a current direction was defined as the direction towards which the currents were flowing. The monthly mean of the current velocity was

Table 2 Measurement periods of currents by V-ADCP and related position (under C1 or B1 buoy) (period time: dd/mm/yyyy).

|	Period start	Period end
Buoy C1	29/08/2012	11/09/2012
	04/10/2012	30/10/2012
	23/11/2012	25/11/2012
Buoy B1	25/11/2012	11/12/2012
	31/12/2012	16/04/2013
	15/06/2013	27/06/2013
	30/06/2013	07/07/2013

calculated at different depths (10, 18, 30, 50, and 70 m) and released as histograms to show the velocity changes with depth during the study period. The data on the current velocity and direction were divided according to the astronomical seasons and plotted in rose diagrams to investigate the seasonal behaviour of the currents and highlight possible prevailing directions.

The meteorological parameters used in this study were measured at the weather station installed on the breakwater of the Giglio Porto harbour (Fig. 1) by the LaMMA (Environmental Modelling and Monitoring Laboratory for Sustainable Development) Consortium of the Region of Tuscany and the Italian Research Council. The weather station provided measurements of sea level [m], mean and maximum wind velocity [m s^{-1}] and prevailing wind and gust direction [°N]. The wind direction was defined as the direction from which the winds were coming. The data were acquired considering a sampling of 10 min.

The weather data were used to support the marine weather bulletin of the Giglio Island activated immediately after the shipwreck. The weather station was composed of a shaft encoder floating hydrometer in a stilling and a 10-m height folding pole with wind velocity and direction sensors (Siap + Micros, S.r.l.) powered by a solar panel. The weather station was 0.5 and 1.2 km from buoys C1 and B1, respectively.

The complete temporal coverage of the data set is shown in Fig. 3.

As was done for the current data, the monthly wind means were also determined, and wind rose diagrams were drawn with the data of the hourly prevailing wind and wind gust.
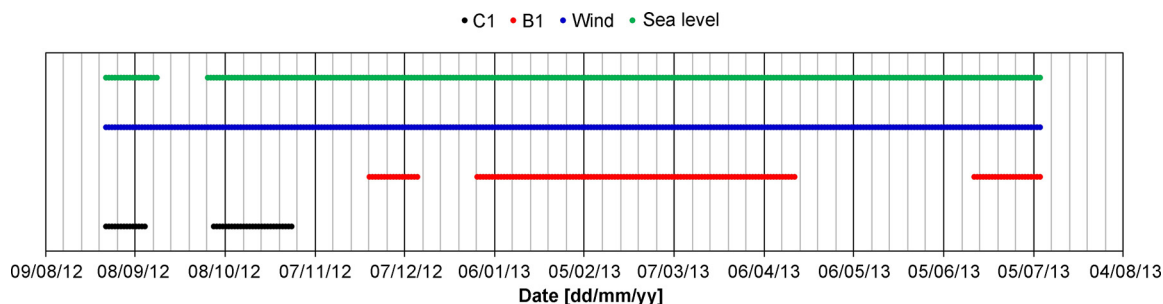
Figure 3 Temporal coverage of current data (under the buoys C1 and B1 in black and red, respectively), wind data (in blue), and sea level data (in green). (For interpretation of the references to color in this figure legend, the reader is referred to the web version of this article.)

Daily sea level means were extracted to highlight the trend of the sea level variations. Tidal harmonic analysis was performed on the hourly sea level data in the period 29th August 2012–7th July 2013, using the Harmgen free software (version 3.1.1, 2006), considering a package of 35 constituents including the four primary harmonic constituents of the semi-diurnal and diurnal frequencies (S2, M2, K1, and O1). Because tidal observations did not cover a full year period, we could not calculate or consider the annual and monthly harmonic components.

A core issue when dealing with time series is determining their pairwise similarity, i.e. the degree to which a given time series resembles another. Therefore, in order to evaluate the presence of possible correlations between the data measured by the V-ADCP (velocity and direction of current) and those provided by the weather station of the LaMMA Consortium (sea level, velocity and direction of wind), a procedure based on the use of the cross-correlation function (CCF) was applied. CCF is a standard method of estimating the degree to which two-time series are similar, and represents a useful measure of strength and direction of the correlation between two random variables (Wei, 2006). In this work, the Normalised Cross-Correlation Function (N-CCF) was considered: it is a popular and easily implemented metric that well follows the rapid changes and the amplitude of two compared signals, and makes it possible to evaluate both the degree of similarity between couples of compared datasets or images and the eventual time shift and delay between two-time series (Tsai et al., 2003; White and Peterson, 1994). N-CCF has found applications in a broad range of the earth sciences such as seismicity, meteorology, and hydrology (Campillo and Paul, 2003; Capello et al., 2016; Mc Millen, 1987; Thouvenot et al., 2016). N-CCF is defined as:

$$\text{N-CCF} = \frac{C_{12}(\tau)}{\sqrt{C_{11}(0)C_{22}(0)}}, \qquad (1)$$

where

$$C_{12}(\tau) = \int_{-\infty}^{+\infty} a_1(t)a_2(t+\tau)dt, \qquad (2)$$

where $a_1(t)$ and $a_2(t)$ are the two time series.

When dealing with digital data, the discrete (or digital) cross-correlation function is used and it is defined as:

$$C_{xv} = \sum_{m=-\infty}^{\infty} x(m)y(m+l), \qquad (3)$$

where $x(m)$ and $y(m)$ are the two discrete-time signals.

The maximum value of the N-CCF (hereafter, the cross-correlation level or similarity level) measures the similarity between signals as a function of the lag of one relative to the other. The maximum correlation is when the maximum N-CCF value is equal to 1, whereas an N-CCF value equal to 0 indicates no correlation between signals.

Before the computation of the N-CCF, the time series data were processed applying the following procedure: (a) resampling to the common frequency of 0.0027778 Hz (the sampling frequency of the V-ADCP data) through an interpolation using a 4th degree polynomial (Scherbaum et al., 1999); (b) extraction of a continuous time window common to both the wind and current series [the period from 15:05 of the 31st December 2012 to 14:00 of the 16th April 2013 was

selected: in this time-period, the complete (without gaps) time series of observations recorded by both V-ADCP and weather station of Giglio Porto were available]; and (c) offset removal (e.g. removing from the time series the average value of all points).

The cross-correlation function was computed in order to assess the possible relationship between: (a) current velocity and direction measured at different depths (10 m and 18 m, 10 m and 30 m, 10 m and 50 m, 10 m and 70 m); (b) wind velocity and current velocity measured at different depths (10 m, 18 m, 30 m, 50 m, and 70 m); (c) prevailing direction of wind and direction of current measured at different depths (10 m, 18 m, 30 m, 50 m, and 70 m); and (d) sea level and current direction measured at 10-m depth.

4. Results

### 4.1. Current variability from moored measurements

The monthly mean current velocities (Fig. 4) show a progressive increase from August 2012 (81 mm s^{-1} in the surface layer at buoy C1) to the autumnal and winter months (251 and 165 mm s^{-1} of maxima measured in the surface layer at buoy B1 in November and December 2012, respectively), with a subsequent decrease in summer 2013 (84 mm s^{-1} in the surface layer at buoy B1). A progressive decrease of current velocity was also visible analysing data from the surface layer (10-m depth) to the bottom layer (70-m depth) in the water column. Below the 50-m depth, the monthly mean current velocity attenuates and the maximum values decrease to values slightly higher than 100 mm s^{-1} (maximum monthly mean value of 136 mm s^{-1} was observed in November at buoy B1).

The maximum current velocity events (velocity > 500 mm s^{-1} at the 10-m depth; Fig. 5) were recorded from the 27th November to the 3rd December 2012 (showing a maximum of 708 mm s^{-1}), on the 6th–7th and on the 18th March 2013 (showing a maximum of 816 mm s^{-1}).

With regard to the current direction, some differences were found among the values measured moving from the surface layer to the bottom in the four seasons. In fact, in the surface layer (10-m depth; Fig. 6a), currents were sharply oriented towards NNW and SSE, whereas moving to the bottom of the water column this effect tended to disappear and the current direction became more widespread (Fig. 6b). Analysing the data recorded at the different depths as a function of the seasons (Fig. 6a and b), it was possible to highlight a seasonal behaviour of current direction. In summer and spring, the prevailing current directions were SE with a smaller portion of NNW directions at the surface (Fig. 6a), while the SSE direction prevails with the greater depth (Fig. 6b). In autumn and winter, the currents are mainly oriented towards NNW in the whole water column, and at 50 and 70-m depths, there is a reversal of the direction with a slight prevalence of SSE near the bottom (Fig. 6b).

4.2. Variability in sea level

The sea level trend shown in Fig. 7 highlights the irregular behaviour shown by the sea level as a function of time. The
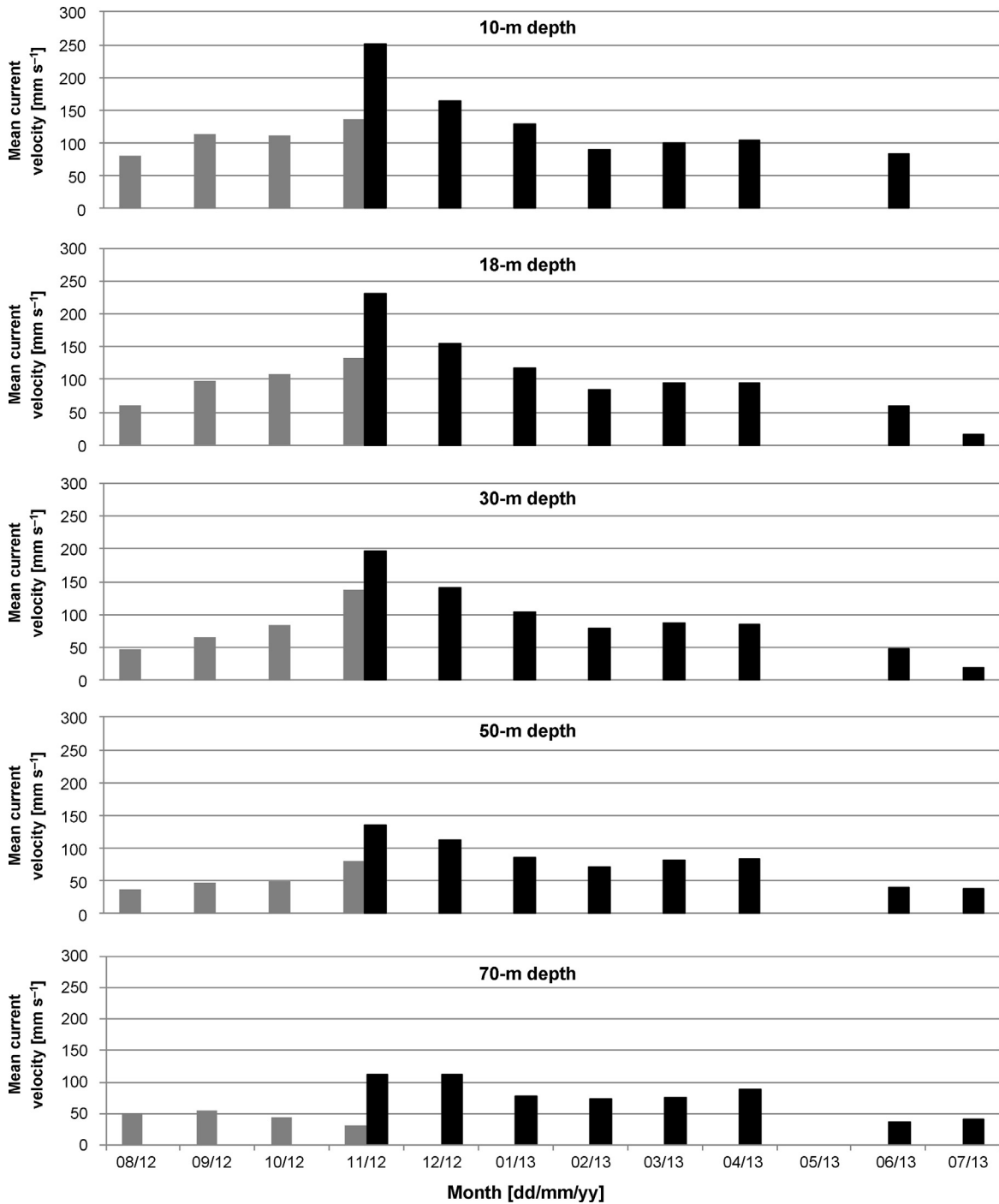
Figure 4 Monthly mean current intensities [mm s^{-1}] measured at 5 different depths in the water column (10, 18, 30, 50, and 70 m) at buoy C1 (grey) and B1 (black). Data of May 2013 are not available as well as data of July 2013 at 10-m depth.

sea level data, recorded at the weather station of Giglio Porto, ranged between −0.33 m and 0.49 m. Two minimum values (−0.31 and −0.33 m) were recorded on the 29th December 2012 and the 28th February 2013 in the presence of a strong N and light SW—SE wind, respectively, and a full moon (28th December 2012 and 26th February 2013). While two positive sea level peaks of 0.41 and 0.49 m (seiches), observed on the 27th and 31st October, respectively, were produced by persistent bad weather conditions, characterised by low atmospheric pressure, a strong SSE

wind, rough seas and heavy precipitation, in conjunction with a full moon (30th October). Maximum sea level variations were recorded in autumn and winter, while minimum variations were observed during late spring and summer.

The main tidal harmonic constituents are reported in Table 3: the main lunar semi-diurnal (M2) prevails over the other constituents with an amplitude of 10.5 cm, four times stronger than the amplitude of the major diurnal constituent (K1).
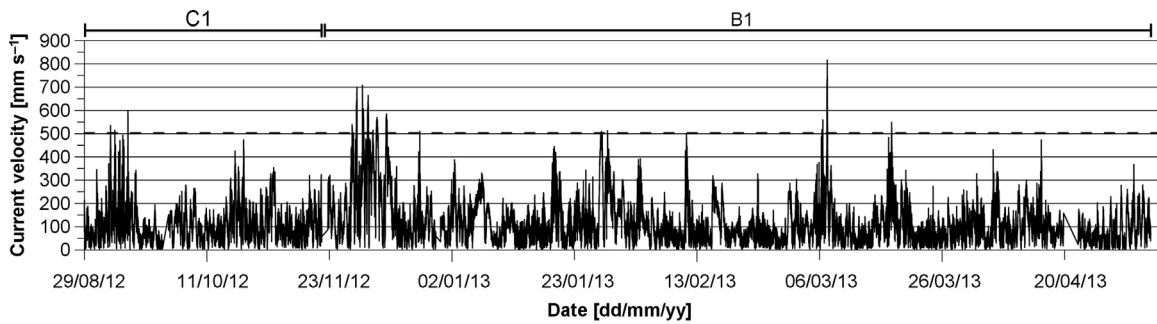
Figure 5   Current velocity distribution measured at 10-m depth during the entire measure period. The dotted line shows the current velocity of 500 mm s^{-1}.

4.3. Seasonal variability in winds

Wind velocity measured at the weather station of Giglio Porto ranged between 0 and 16.6 m s^{-1} and showed a monthly mean of 3.2 m s^{-1} in summer and of 4.9 m s^{-1} in winter (Fig. 8). Considering only the case of wind velocities higher than the mean value of the near gale velocities (15 m s^{-1}) according to the Beaufort Scale, only five events of significant wind were recorded in autumn and winter. The highest wind velocity was recorded on the 11th November 2012 during a robust anticyclonic front characterised by SE-oriented winds.

The rose diagrams (Fig. 9) reporting wind measurements show that winds originate mostly from two directions, SE and NNW; the strongest winds come from the SE. A SW wind direction is also visible mainly looking at the wind gusts diagram.

It is also possible to note some seasonal variation in the wind direction; in summer, winds come mainly from the NNW; in autumn, the predominant origin direction is the SE; in winter, the strongest winds come from the SE, whereas weaker winds come from the NW; in spring, the two prevailing directions (NNW and SE) are present, with a slight prevalence of the SE direction.

5. Data correlation results

Fig. 10 shows the results of the Normalised Cross-Correlation Function (N-CCF; Eq. (1)) obtained considering current velocities measured at different depths (Fig. 10a) and those resulting from correlating wind velocities and current velocities measured at different depths (Fig. 10b).

The time series of current velocities measured at different depths (Fig. 10a) exhibit a similarity level, which tends to decrease as the difference between measuring depth increases (y-axis of Fig. 10a); in fact, the cross-correlation level between the current velocity values measured at the 10-m depth and those measured at the 18-m depth is equal to 0.82, whereas for the data measured at the 10-m depth and at the 70-m depth the similarity decreases to 0.36.

It should be noted that the time shift (x-axis of Fig. 10a) in current velocity values measured at different depths changes too. Data measured at the 10-m depth and the 18-m depth are not phase-shifted, whereas the time shift between data measured at the10-m depth and the 70-m depth is equal to about 1 h and 30 min (~1.5 h). Similar results are obtained by evaluating the similarity level between current directions measured at different depths (not showed in Fig. 10).

Between directions measured at the10-m depth and those measured at the 18-m depth it is possible to observe 0.52 of similarity, while the similarity decreases to 0.16 when the data of the 10-m depth were compared to the data of the 70-m depth.

The correlation between the wind and current (time series) was extremely low (Fig. 10b). It was lower than 0.20 for the velocity data (Fig. 10b) and 0.10 for the direction data. This result shows that the wind does not seem to be related to the current velocity or rather the wind does not significantly influence the velocity and direction of the current.

In order to better investigate the correlation between the wind and current, a further analysis was performed estimating the N-CCF between wind velocity and current velocity measured at the 10-m depth for three events characterised by a wind velocity peak greater than 15 m s^{-1} (the mean velocity of the near gale wind; Figs. 11—13). In particular, three sub-windows with duration of approximately five days, around the 12th February 2013, the 7th March 2013, and the 18th March 2013, were analysed. Considering only these events, the correlation between the wind and current velocity significantly increased with respect to the previous analysis (performed considering the entire recording period), showing similarity levels greater than 0.50 (panel c in Figs. 11—13). The time shift between the wind and current velocities was very different in the three different cases. In fact, in the first case (Fig. 11), the time shift was equal to 4 h ca, in the second case (Fig. 12) it was 21 h, and in the third case it was 12 h ca (Fig. 13).

Other important experimental evidence concerns the relationship between the wind and current direction observed during these three events. In correspondence of maximum values of the wind and current velocity (highlighted in Figs. 11—13 by the dashes), a relationship between a SSE wind (e.g. "Scirocco" 135°—180°) and a N current is visible. It must be noted that the events of strong wind extrapolated from the study period are all analogous, that is all come mainly from the SSE, and therefore, it is not possible to analyse other cases of strong winds with different directions. In Figs. 11—13 (panels b and e), it is possible to note an inversion of the current direction at the end of the wind action and the consequently variation in the current velocity: the current direction switches suddenly from the NW to the SE as if the system unbends at the forcing end.

The last analysis has been performed computing the N-CFF between the sea level data and the current direction measured at the 10-m depth. These two signals appear uncorrelated (similarity level lower than 0.10).
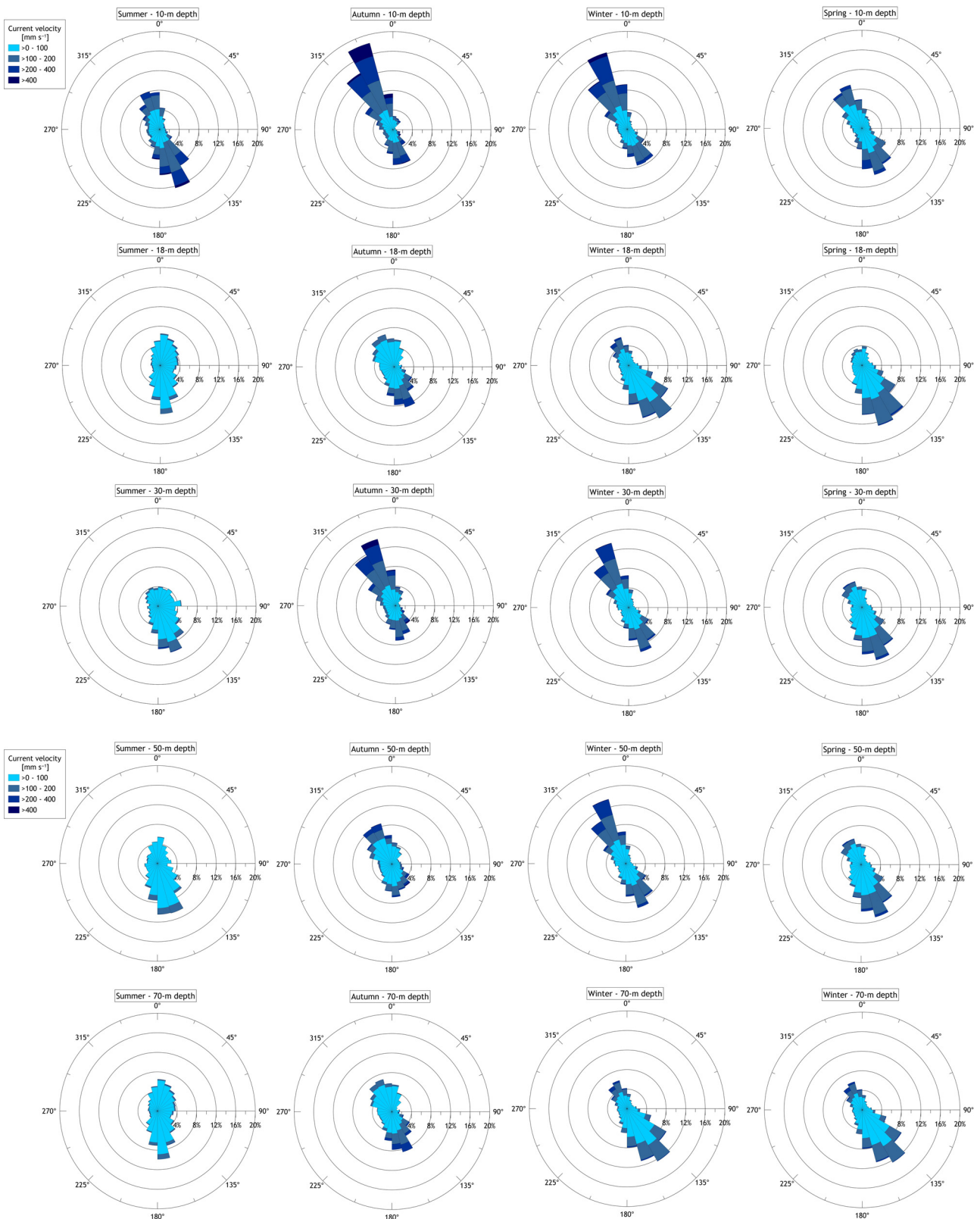
Figure 6 (a) Seasonal diagrams of current velocity and direction distribution measured at 10, 18 and 30-m depth from the 28th August 2012 to the 7th July 2013. Current direction, following oceanographic convention, is the direction to which the currents are going. (b) Seasonal diagrams of current velocity and direction distribution measured at 50 and 70-m depth from the 28th August 2012 to the 7th July 2013. Current direction, following oceanographic convention, is the direction to which the currents are going.

Table 3 Tidal semi-diurnal and diurnal harmonic constituents (M2, S2, K1, and O1) of Giglio Porto expressed in amplitude (in cm) and phase (in degree, °) and calculated between 29/08/2012 and 07/07/2013.

This study (Giglio Porto, Italy)	M2	S2	K1	O1
Period 29/08/2012—07/07/2013	10.5 cm, 258°	3.8 cm, 279°	2.6 cm, 199°	1.3 cm, 121°
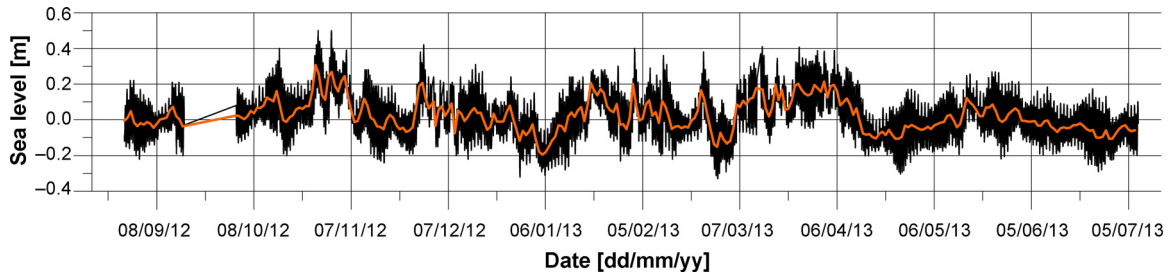
Figure 7 Hourly (in black) and daily mean (in orange) sea level [m] measurements recorded at the weather station of Giglio Porto between August 2012 and July 2013. (For interpretation of the references to color in this figure legend, the reader is referred to the web version of this article.)
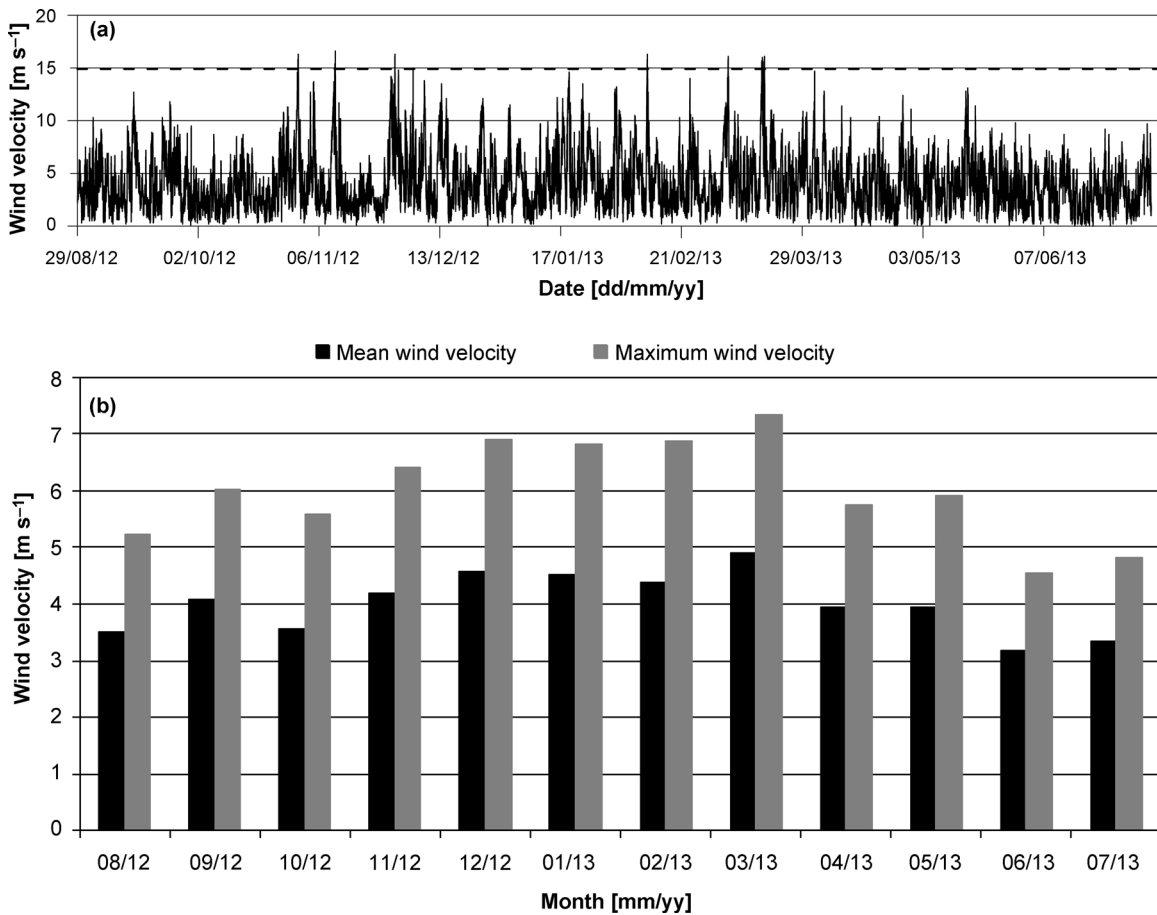
Figure 8 Top panel: wind velocity measured at Giglio Porto between August 2012 and July 2013; the black dash line shows the mean value of the near gale wind (15 m s^{-1}). Bottom panel: monthly mean (black) and maximum (grey) values of wind velocity [m s^{-1}].
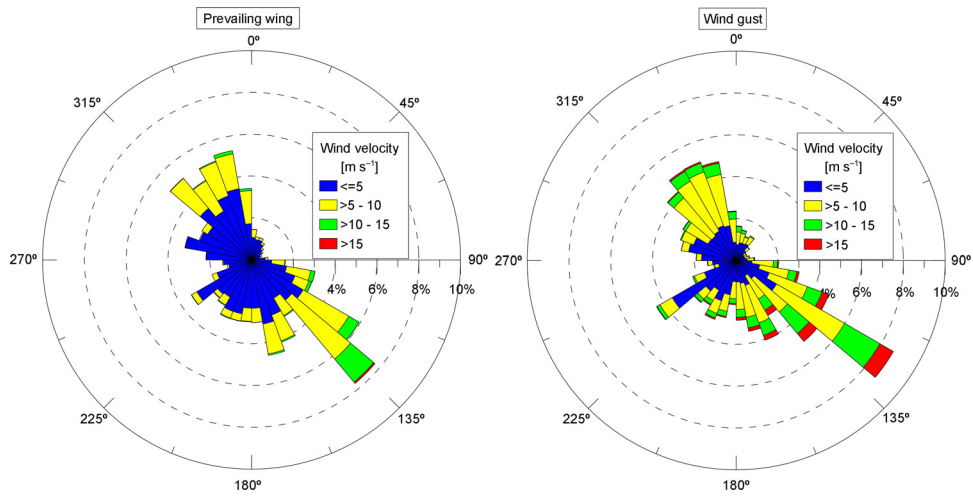
Figure 9   Rose diagrams showing the velocity and the direction of prevailing wind (left panel) and the maximum velocity and direction of gusts (right panel). The wind direction is here defined as the direction from which the wind is coming. Data are measured every 10 min at the weather station of Giglio Porto during the study period.

6. Discussion

The irregular trend of the sea level measured at the weather station of Giglio Porto highlighted the combined action of meteorological forcing (autumn-winter waves, atmospheric pressure and winds) and the astronomical tidal components (Earth-Moon-Sun gravitational relationship). Tidal amplitude was in accordance with the general range of the Tyrrhenian Sea (Alberola et al., 1995; Ferrarin et al., 2013). The main

tidal harmonic constituents found at Giglio Porto retraced the values found by both Polli (1955) at Civitavecchia harbour (Lazio, central Tyrrhenian Sea) and Androsov et al. (2002) at the Scylla station (northern Strait of Messina, Sicily, southern Tyrrhenian Sea) in both amplitude and phase, although our data set did not cover a full year. On the contrary, the Giglio Porto constituents were significantly different from those found in other seas (such as the Adriatic Sea; Janeković and Kuzmíc, 2005) or the Atlantic Ocean (Fanjul et al., 1997) due
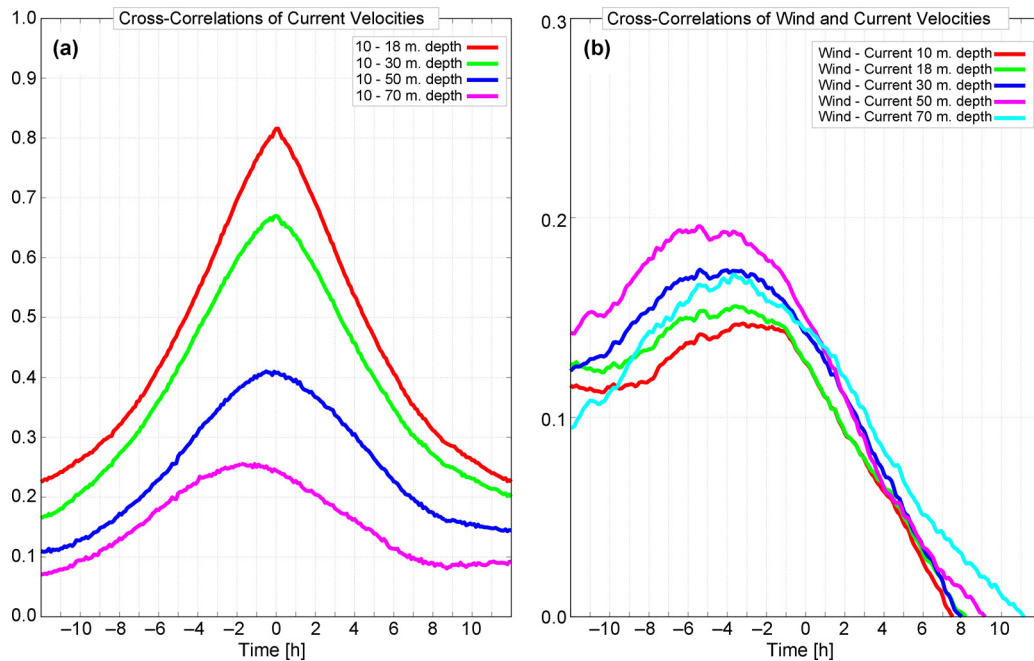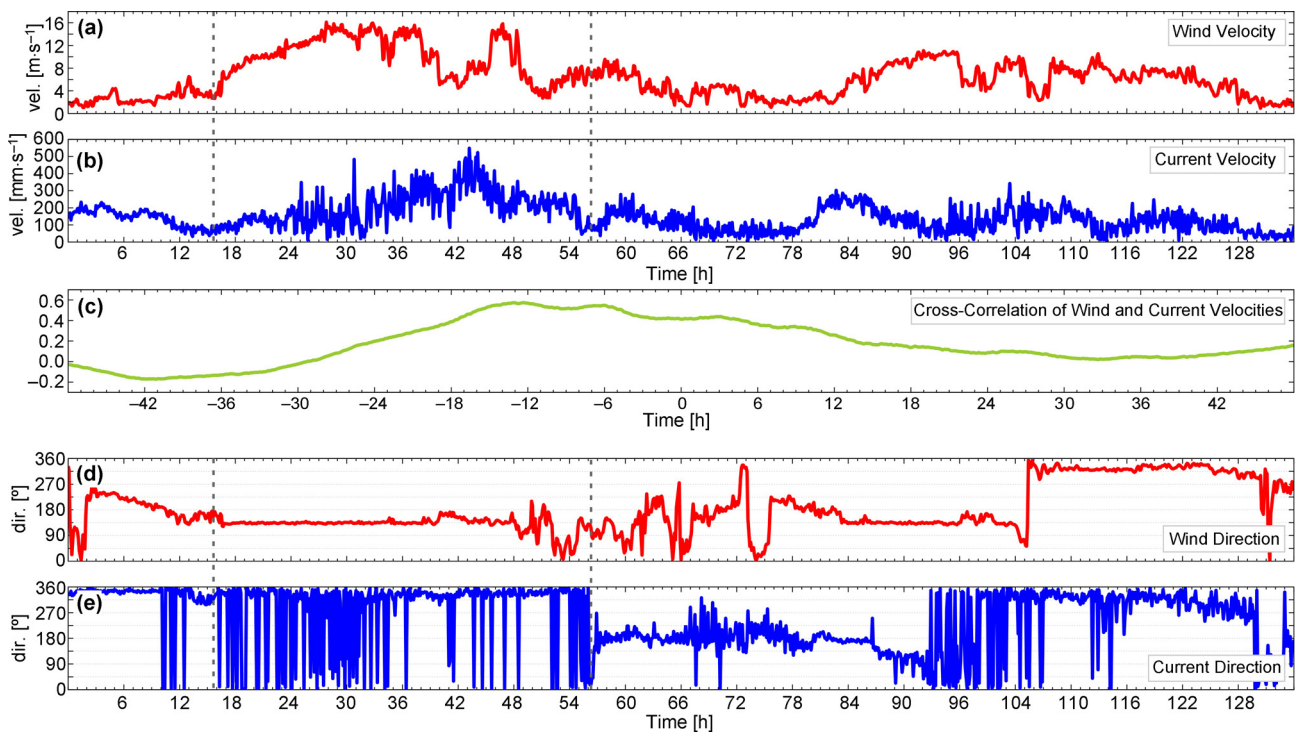

Figure 10   Normalised Cross-Correlations (N-CCF) obtained considering (a) current velocity measured at different depth [current measured at 10 and 18 m (red), 10 and 30 m (green), 10 and 50 m (blue), and 10 and 70 m (pink)], and (b) wind velocity and current velocity measured at different depth [10 m (red), 18 m (green), 30 m (blue), 50 m (pink), and 70 m (cyan)] in the whole period. Values are expressed in a 0—1 scale (*y*-axis), where 1 corresponds to the perfect correlation level, and 0 to the absence of correlation. The *y* scale of panel b is zoomed to 0.3 to better show the results. (For interpretation of the references to color in this figure legend, the reader is referred to the web version of this article.)
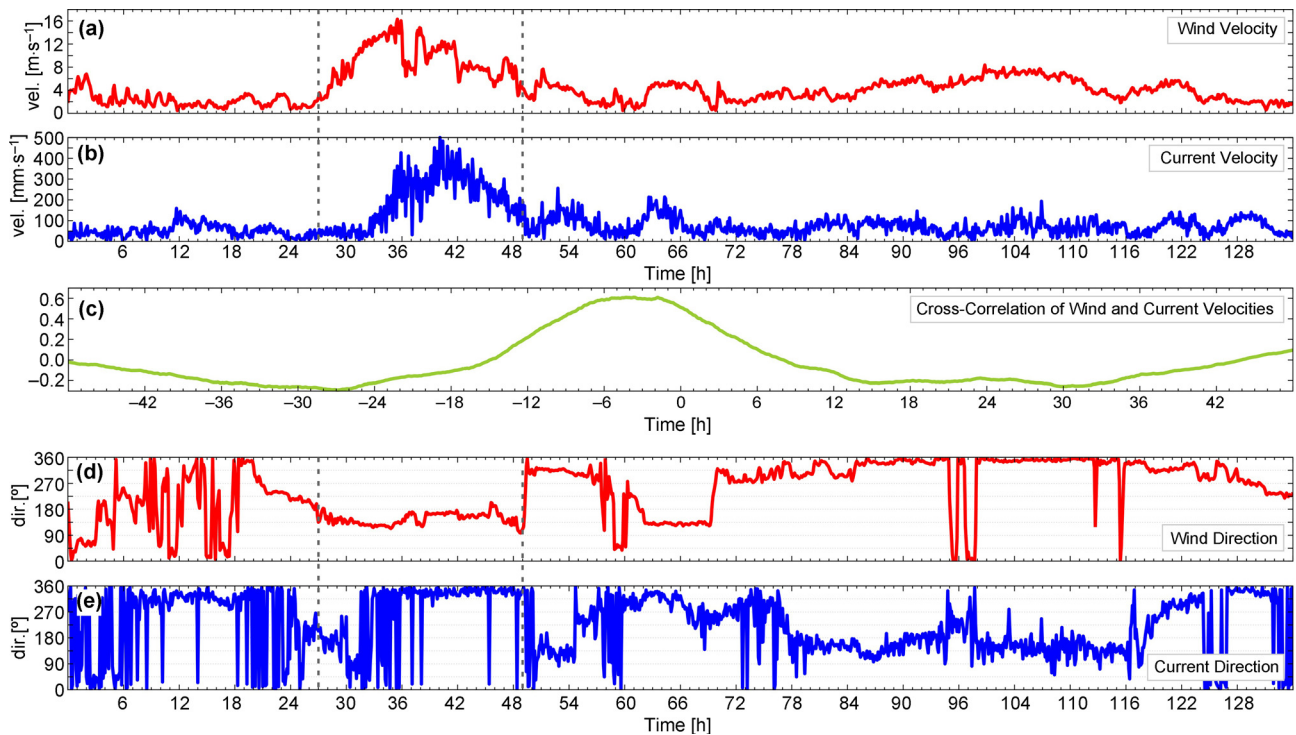
Figure 11 Analysis of the relation between wind and current during the period 9th—15th February 2013. (a) Wind velocity data, (b) current velocity data measured at 10 m depth, (c) Normalised Cross-Correlation Function (N-CCF) obtained considering wind and current velocity at 10-m depth, (d) wind direction data, and (e) current direction data at 10-m depth.
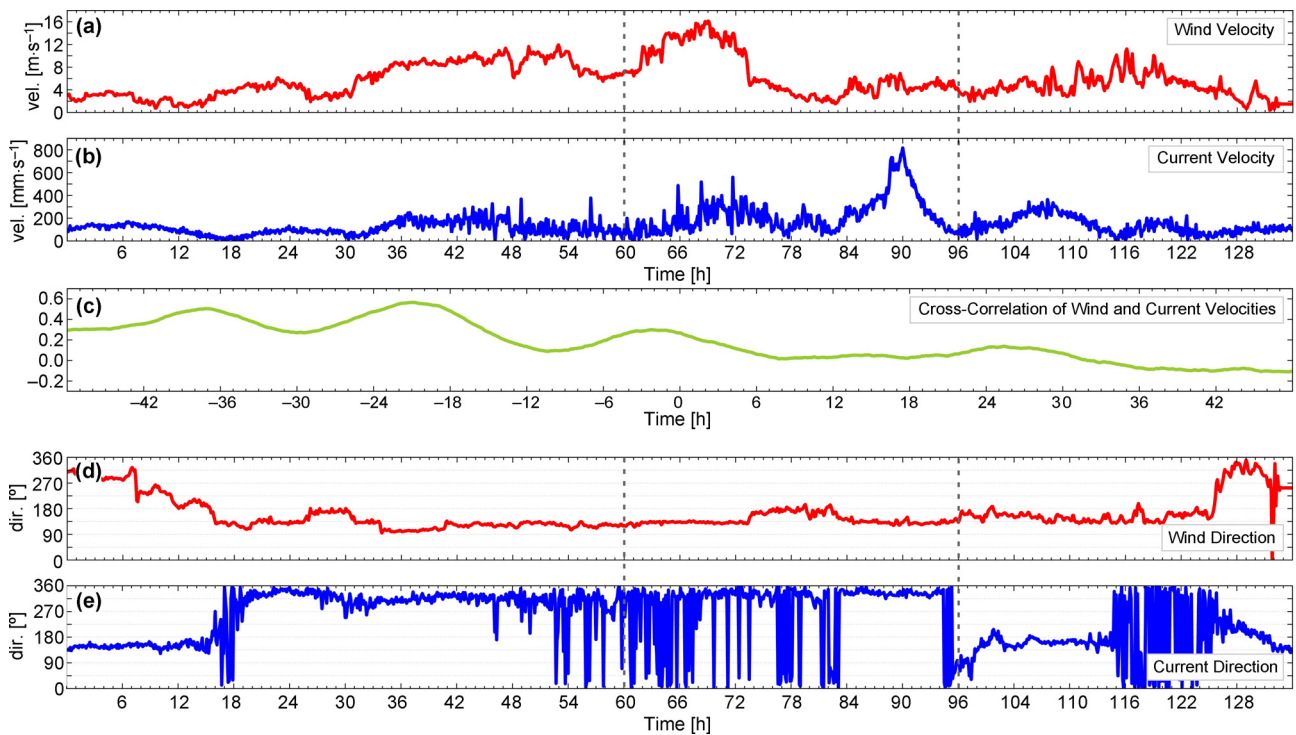
Figure 12 Analysis of the relation between wind and current during the period 3rd—9th March 2013. (a) Wind velocity data, (b) current velocity data measured at 10 m depth, (c) Normalised Cross-Correlation Function (N-CCF) obtained considering wind and current velocity at 10-m depth, (d) wind direction data, and (e) current direction data at 10-m depth.

Figure 13 Analysis of the relation between wind and current during the period 16th—22nd March 2013. (a) Wind velocity data, (b) current velocity data measured at 10 m depth, (c) Normalised Cross-Correlation Function (N-CCF) obtained considering wind and current velocity at 10-m depth, (d) wind direction data, and (e) current direction data at 10-m depth.

to the different characteristics and dynamics that influence these water basins.

The results found in the area under study retrace the well known surface circulation characterised by the predominant movement of the water masses along a NW—SE direction (Schroeder et al., 2011), corresponding to the NNW—SSE orientation of the major axis of the Giglio Island and the channel between the island and the mainland (western coast of the Italian peninsula). This characteristic of the flow is evidence of the importance of the topography and morphology of the area (presence of islands, canyons, headlands, etc.) on the current regime (Gravili et al., 2001). The predominance of NW currents in winter and autumn is also induced by the corresponding overall cyclonic Tyrrhenian circulation (Iermano et al., 2016), whereas the frequent inversions of current direction in summer and spring may be related to episodes of Tyrrhenian current reversal (Gravili et al., 2001).

The inter-seasonal and daily variations in both velocity and direction of currents confirm the short period variability of the flow already found in the Tyrrhenian basin on a greater scale by Pierini and Simioli (1998), and subjected to study as a distinctive feature of oceanic basins.

The study of the interactions between external forcing processes and water mass circulation is typically carried out with numerical model simulations (Dumas et al., 2012; Lovato et al., 2010; Molcard et al., 2002; Pierini and Simioli, 1998) or the application, for example, of the Fourier or Wavelet transforms (Fontán et al., 2009; Lovato et al., 2010). The use of the NCCF in our case allowed us to highlight some of the main characteristics of the current structure and

behaviour in relation to external forcing. In fact, the decreasing similarity level in velocity and direction and the time shift in the currents with increasing depth can be evidence of both Ekman's theory (Bjerknes, 1964) and the time necessary for a boundary-forcing current to make a local barotropic adjustment (Gravili et al., 2001).

In general, as in the case of currents, the prevailing wind directions were shown to agree with the NNW-SSE orientation of the island's major axis and also the position of the weather station on the breakwater of Giglio Porto that is protected from winds from the western quadrants by the presence of the island. The direction (NNW-SSE) of the dominant wind is seasonally variable over the Giglio Island shelf, in accordance with the circulation (with opposite directions), as happens in the entire Tyrrhenian Sea (Pierini and Simioli, 1998). Nevertheless, on a long-time scale, the winds and currents do not seem to be correlated parameters in term of velocity and direction, as found in other cases on the continental shelf (e.g. south-eastern Australia; Wood et al., 2016). This condition is the opposite of what was found, for example by Lentz (2007) and Liu and Weisberg (2012), on the Middle Atlantic Bight and West Florida continental shelves, respectively, where the winds are seasonally consistent and generate steady seasonal responses in the circulation. Our results were also in contrast with what was found by Chen et al. (1996) over the Texas-Louisiana shelf, where the correlation between the along-shore currents and wind stress increases close to the coast. In addition to the wind behaviour, these differences can derive from the morphology of the shelf and the coasts and the effect of the prevailing large-scale circulation (Fontán et al., 2009; Liu and Weisberg,

2012; Wood et al., 2016), such as in our case the general Tyrrhenian circulation affects the current measured at the Giglio Porto buoy.

However, strong wind episodes (velocity > 15 m s^{-1}) over a limited period of observation seem to be able to influence the current velocity pattern creating a cause-effect relationship that prevails in the action of the Tyrrhenian circulation. As already found by Li et al. (2014) in the Gulf of Maine (U.S.A.), the mean coastal current centred near the 100-m isobath can deviate fairly frequently due to effects of wind forcing and small-scale baroclinic structures. The effect of a strong wind on current velocity could be also be facilitated by the homogeneity of the water column; in fact, all the three cases studied took place in winter, when the water column was not yet stratified by the spring and summer warming of the atmosphere (Iermano et al., 2016).

Starting from the elaboration reported in Figs. 11—13, it was noted that without external forcing (e.g. strong wind), near the coast, the current direction reverses by 180° (e.g. counter-current) with respect to the Tyrrhenian flux, while on the occasion of a strong wind from the SE, also near the coast, the current direction alters to the North. This condition was also noted by Gravili et al. (2001) in the Gulf of Naples (south-eastern Tyrrhenian Sea), where a two-day interval of NW flow was followed by a rapid linear transition to an opposite flux.

The sea level and the current direction are not correlated, confirming the low influence of this phenomenon on the water masses in the Tyrrhenian basin, at least at the short distance from the coast that the buoy was located (Clarke and Battisti, 1981). Both the irregular sea level trend and the prevalence of the semi-diurnal M2 constant on the major diurnal constituents supports the argument that the tide does not have an evident and quantifiable (with the cross-correlation use) effect on the current. Therefore, the sea level is influenced by both the general Tyrrhenian circulation and the influence of the wind, phenomena of high intensity and long duration.

7. Conclusions

Thanks to the monitoring plan carried out during the removal operation of the Costa Concordia wreck at Giglio Island (Italy), in situ observations (August 2012—July 2013), including continuous current measurements and wind and sea level recordings, were used to study the variability of these phenomena near the island coasts in the Tyrrhenian basin.

The results showed a significant inter-seasonal variability in both local wind and current velocity, and also in their directions despite the fact that they are mainly forced to move in a NW—SE direction by the presence of the island. The currents are principally dominated by the general Tyrrhenian circulation, and only partially affected by the wind (only in strong wind cases), while the sea level has no effects on the current regime due to its low intensity.

The N-CCF is a metric commonly used to evaluate the degree of similarity between two signals, and is usually applied to seismic, hydrological and meteorological studies in the Earth sciences, but it seems to be a useful tool for oceanographic studies and analysis of the physical processes driving the local circulation and the relationship with forcing factors. In fact, our contribution, with the N-CCF applied to the influence of the boundary forcing (wind and sea level) on the currents, provided evidence that can highlight and explain cause-effect relationships such as, for example, in the case of the high levels of correlation found between strong SE winds and currents or the absence of a correlation between currents and sea level.

Within this context, further analysis will be necessary to investigate the correlation level between currents and other directions of strong winds (e.g. NE and SW) measured at the Giglio Island to analyse the behaviour of the currents to these types of stress. Furthermore, the application of this method to other study cases in other locations with different oceanographic characteristics will allow us to confirm the usefulness of the N-CCF in oceanographic studies.

Acknowledgments

References

Alberola, C., Rousseau, S., Millot, C., Astraldi, M., Font, J., Garcia-Lafuente, J., Gasparini, G.P., Send, U., Vangriesheim, A., 1995. Tidal currents in the western Mediterranean Sea. Oceanol. Acta 18 (2), 273—284.

Androsov, A.A., Kagan, B.A., Romanenkov, D.A., Voltzinger, N.E., 2002. Numerical modelling of barotropic tidal dynamics in the strait of Messina. Adv. Water Resour. 25 (4), 401—415, http://dx.doi.org/10.1016/S0309-1708(02)00007-6.

Astraldi, M., Gasparini, G.P., 1994. The seasonal characteristics of the circulation in the Tyrrhenian Sea. In: La Viollette, P.E. (Ed.), Seasonal Interannual Variability of the Western Mediterranean Sea. Am. Geophys. Union, Washington, DC, 115—134, http://dx.doi.org/10.1029/CE046p0115.

Bjerknes, J., 1964. Atlantic air—sea interaction. In: Landsberg, H.E., Van Mieghem, J. (Eds.), Advances in Geophysics. Academic Press, New York/London, 1—81.

Bolaños, R., Tornfeldt Sørensen, J.V., Benetazzo, A., Carniel, S., Sclavo, M., 2014. Modelling ocean currents in the northern Adriatic Sea. Cont. Shelf Res. 87, 54—72, http://dx.doi.org/10.1016/j.csr.2014.03.009.

Campillo, M., Paul, A., 2003. Long-range correlations in the diffusion seismic coda. Science 299 (5606), 547—549, http://dx.doi.org/10.1126/science.1078551.

Capello, M., Cutroneo, L., Ferretti, G., Gallino, S., Canepa, G., 2016. Changes in the physical characteristics of the water column at the mouth of a torrent during an extreme rainfall event. J. Hydrol. 541 (Pt. A), 146—157, http://dx.doi.org/10.1016/j.jhydrol.2015.12.009.

Cazenave, A., Bonnefond, P., Mercier, F., Dominh, K., Toumazou, V., 2002. Sea level variations in the Mediterranean Sea and Black Sea from satellite altimetry and tide gauges. Global Planet. Change 34 (1—2), 59—86, http://dx.doi.org/10.1016/S0921-8181(02)00106-6.

Chen, C., Reid, R.O., Nowlin Jr., W.D., 1996. Near-inertial oscillations over the Texas—Louisiana shelf. J. Geophys. Res. 101 (C2), 3509—3524.

Clarke, A.J., Battisti, D.S., 1981. The effect of continental shelves on tides. Deep-Sea Res. 28A (7), 665—682.

Dumas, F., Le Gendre, R., Thomas, Y., Andréfouët, S., 2012. Tidal flushing and wind driven circulation of Ahe atoll lagoon (Tuamotu Archipelago, French Polynesia) from in situ observations and numerical modelling. Mar. Pollut. Bull. 65 (10—12), 425—440, http://dx.doi.org/10.1016/j.marpolbul.2012.05.041.

Fanjul, E.A., Gomez, B.P., Sanchez-Arevalo, I.R., 1997. A description of the tides in the Eastern North Atlantic. Prog. Oceanogr. 40 (1—4), 217—244, http://dx.doi.org/10.1016/S0079-6611(98)00003-2.

Ferrarin, C., Roland, A., Bajo, M., Umgiesser, G., Cucco, A., Davolio, S., Buzzi, A., Malguzzi, P., Drofa, O., 2013. Tide-surge-wave modelling and forecasting in the Mediterranean Sea with focus on the Italian coast. Ocean Model. 61, 38—48, http://dx.doi.org/10.1016/j.ocemod.2012.10.003.

Fontán, A., González, M., Wells, N., Collins, M., Mader, J., Ferrer, L., Esnaola, G., Uriarte, A., 2009. Tidal and wind-induced circulation within the Southeastern limit of the Bay of Biscay: Pasaia Bay. Basque Coast. Cont. Shelf Res. 29 (8), 998—1007, http://dx.doi.org/10.1016/j.csr.2008.12.013.

Frezza, V., Carboni, M.G., 2009. Distribution of recent foraminiferal assemblages near the Ombrone River mouth (Northern Tyrrhenian Sea, Italy). Rev. Micropléontol. 52 (1), 43—66, http://dx.doi.org/10.1016/j.revmic.2007.08.007.

Gravili, D., Napolitano, E., Pierini, S., 2001. Barotropic aspects of the dynamics of the Gulf of Naples (Tyrrhenian Sea). Cont. Shelf Res. 21 (5), 455—471, http://dx.doi.org/10.1016/S0278-4343(00)00100-X.

Halverson, M.J., 2014. Atmospheric and tidal forcing of the exchange between Prince William Sound and the Gulf of Alaska. Dyn. Atmos. Ocean. 65, 86—106, http://dx.doi.org/10.1016/j.dynatmoce.2013.12.001.

Iermano, I., Moore, A.M., Zambianchi, E., 2016. Impacts of 4-dimensional variational data assimilation in a coastal ocean model of southern Tyrrhenian Sea. J. Mar. Syst. 154 (Pt. B), 157—171, http://dx.doi.org/10.1016/j.jmarsys.2015.09.006.

Janeković, I., Kuzmić, M., 2005. Numerical simulation of the Adriatic Sea principal tidal constituents. Ann. Geophys. 23, 3207—3218.

Lentz, S.J., 2007. Seasonal variations in the circulation over the Middle Atlantic Bight continental shelf. J. Phys. Oceanogr. 38, 1486—1500, http://dx.doi.org/10.1175/2007JPO3767.1.

Li, Y., He, R., McGillicuddy Jr., D.J., 2014. Seasonal and interannual variability in Gulf of Maine hydrodynamics: 2002—2011. Deep-Sea Res. 103 (Pt. II), 210—222, http://dx.doi.org/10.1016/j.dsr2.2013.03.001.

Liu, Y., Weisberg, R.H., 2012. Seasonal variability on the West Florida Shelf. Prog. Oceanogr. 104, 80—98, http://dx.doi.org/10.1016/j.pocean.2012.06.001.

Lovato, T., Androsov, A., Romanenkov, D., Rubino, A., 2010. The tidal and wind induced hydrodynamics of the composite system Adriatic Sea/Lagoon of Venice. Cont. Shelf Res. 30 (6), 692—706, http://dx.doi.org/10.1016/j.csr.2010.01.005.

Mc Millen, R.T., 1987. An eddy correlation technique with extended applicability to non-simple terrain. Bound.-Lay Meteorol. 43 (3), 231—245, http://dx.doi.org/10.1007/BF00128405.

Millot, C., Taupier-Letage, I., 2005. Circulation in the Mediterranean Sea. Handb. Environ. Chem. 5 (Pt K), 29—66, http://dx.doi.org/10.1007/b107143.

Molcard, A., Pinardi, N., Iskandarani, M., Haivogel, D.B., 2002. Wind driven general circulation of the Mediterranean Sea simulated with a Spectral Element Ocean Model. Dyn. Atmos. Ocean. 35 (2), 97—130, http://dx.doi.org/10.1016/S0377-0265(01)00080-X.

Mosetti, F., Purga, N., 1982. First results on long- and midperiod tide distribution in Italian seas and their existence in the groundwater. Il Nuovo Cimento 5C (2), 143—158.

Naranjo, C., Garcia-Lafuente, J., Sannino, G., Sanchez-Garrido, J.C., 2014. How much do tides affect the circulation of the Mediterranean Sea? From local processes in the Strait of Gibraltar to basin-scale effects. Prog. Oceanogr. 127, 108—116, http://dx.doi.org/10.1016/j.pocean.2014.06.005.

Pierini, S., Simioli, A., 1998. A wind-driven circulation model of the Tyrrhenian Sea area. J. Mar. Syst. 18, 161—178.

Polli, S., 1955. Variazioni delle costanti armoniche delle maree col livello del mare. Ann. Geofis. 8 (2), 202—207.

Rossetti, F., Faccenna, C., Jolivet, L., Funiciello, R., Tecce, F., Brunet, C., 1999. Syn- versus post-orogenic extension: the case of Giglio Island (Northern Tyrrhenian Sea, Italy). Tectonophysics 304 (1—2), 71—93, http://dx.doi.org/10.1016/S0040-1951(98)00304-7.

Scherbaum, F., Johnson, J., Rietbrock, A., 1999. PITSA (Programmable Interactive Toolbox for Seismological Analysis). PITSA Users Manual, 222 pp.

Schroeder, K., Haza, A.C., Griffa, A., Özgökmen, T.M., Poulain, P.M., Gerin, R., Peggion, G., Rixen, M., 2011. Relative dispersion in the Liguro-Provençal basin: from sub-mesoscale to mesoscale. Deep-Sea Res. Pt. I 58 (3), 209—228, http://dx.doi.org/10.1016/j.dsr.2010.11.004.

Thouvenot, F., Jenatton, L., Scafidi, D., Turino, C., Potin, B., Ferretti, G., 2016. Encore ubaye: earthquake swarms, foreshocks, and aftershocks in the Southern French Alps. Bull. Seismol. Soc. Am. 106 (5), 2244—2257, http://dx.doi.org/10.1785/0120150249.

Tsai, D.M., Lin, C.T., Chen, J.F., 2003. The evaluation of normalized cross correlations for defect detection. Pattern Recogn. Lett. 24 (15), 2525—2535, http://dx.doi.org/10.1016/S0167-8655(03)00098-9.

Tsimplis, M., Spada, G., Marcos, M., Flemming, N., 2011. Multi-decadal sea level trends and land movements in the Mediterranean Sea with estimates of factors perturbing tide gauge data and cumulative uncertainties. Global Planet. Change 76 (1—2), 63—76, http://dx.doi.org/10.1016/j.gloplacha.2010.12.002.

Vetrano, A., Napolitano, E., Iacono, R., Schroeder, K., Gasparini, G.P., 2010. Tyrrhenian Sea circulation and water mass fluxes in spring 2004: observations and model results. J. Geophys. Res. 115, C06023, http://dx.doi.org/10.1029/2009JC005680.

Wei, W.W.S., 2006. Time Series Analysis, Univariate and Multivariate Methods, 2nd ed. Addison-Wesley, Boston, MA, 614 pp.

White, R.J., Peterson, B.M., 1994. Comments on cross-correlation methodology in variability studies of active galactic nuclei. Publ. Astron. Soc. Pac. 106 (702), 879—889.

Wood, J.E., Schaeffer, A., Roughan, M., Tate, P.M., 2016. Seasonal variability in the continental shelf waters off southeastern Australia: fact or fiction? Cont. Shelf Res. 112, 92—103, http://dx.doi.org/10.1016/j.csr.2015.11.006.